Inorganic Chemistry
Article

Inorg. Chem. **2009**, *48*, 7127–7140 **7127**
DOI: 10.1021/ic9002127

Theoretical Study of Dioxygen Induced Inhibition of [FeFe]-Hydrogenase

Martin T. Stiebritz and Markus Reiher*

Laboratorium für Physikalische Chemie, ETH Zurich, Wolfgang-Pauli-Strasse 10 8093 Zürich, Switzerland

Received February 2, 2009

Hydrogenases comprise a variety of enzymes that catalyze the reversible oxidation of molecular hydrogen. Out of this group, [FeFe]-hydrogenase shows the highest activity for hydrogen production which is, therefore, of great interest in the field of renewable energies. Unfortunately, this comes with the flaw of a generally very high sensitivity against molecular oxygen that irreversibly inhibits this enzyme. While many studies have already addressed the mechanism of hydrogen formation by [FeFe]-hydrogenase, little is kown about the molecular and mechanistic details leading to enzyme inactivation by O_2. In order to elucidate this process, we performed density functional theory calculations on several possible O_2 adducts of the catalytic center — the so-called H-cluster — and show that the direct interaction of the $[2Fe]_H$ subsite with dioxygen is an exothermic and specific reaction in which O_2 most favorably binds in an end-on manner to the distal Fe_d. Based on the results, we propose a protonation mechanism that can explain the irreversibility of dioxygen-induced enzyme inactivation by water release and degradation of the ligand environment of the H-cluster.

1. Introduction

In biological systems the reversible oxidation of molecular hydrogen is catalyzed by the diverse class of hydrogenases. These enzymes are found in many different microorganisms and can be divided into three groups according to the metal composition of their active sites[1]—[FeFe]-hydrogenase, [NiFe]-hydrogenase, and H_2-forming methylenetetrahydromethanopterin dehydrogenase (Hmd). Because of their ability to catalyze the formation of molecular hydrogen, these enzymes are attractive candidates in the field of renewable energies. In this regard, [FeFe]-hydrogenase is of particular interest because only this enzyme shows a high activity not only for hydrogen oxidation but also for hydrogen production, i.e., H^+ reduction.[2] Its inhibition by dioxygen,[2,3] however, represents a considerable drawback for possible applications in hydrogen production facilities and fuel cells. The sensitivity of [FeFe]-hydrogenase against O_2 varies depending on the species background (i.e., in which organism it occurs). Whereas the enzyme from *Clostridium pasteurianum* can only be purified under anaerobic conditions,[4] the *Desulfovibrio vulgaris* enzyme can be isolated as an inactive oxygen tolerant form which, after a reductive activation process, becomes sensitive against O_2.[5,6] Electrochemical characterization experiments on the enzyme from *Clostridium acetobutylicum* suggest that irreversible O_2-induced inhibition most likely involves the degradation of the active center after the initial reversible formation of an oxygen-bound intermediate.[7] In sharp contrast, [NiFe]-hydrogenases are inhibited in a more reversible manner by dioxygen and can be reactivated by reduction.[2] Additionally, variants of this enzyme form were identified in *Ralstonia eutropha* that show elevated oxygen tolerance. Structural studies revealed amino acid substitutions in the gas diffusion channel of the enzyme that explain this property by an impeded diffusion of O_2 due to steric hindrance.[8] So far, no comparable mutants were isolated from the species that harbor [FeFe]-hydrogenases, but it should be possible to obtain them, e.g., by protein engineering. However, because of the irreversibility of the inhibition process, it is not clear whether this approach could protect the active center from oxygen-induced destruction.

It is, therefore, mandatory to gain deeper insight into the chemistry of oxygen inhibition of [FeFe]-hydrogenase in order to better understand the inactivation mechanism and to be able to possibly design more oxygen tolerant enzyme variants. Whereas many studies have addressed the catalytic

*To whom correspondence should be addressed. E-mail: markus.reiher@phys.chem.ethz.ch.

(1) Vignais, P. M.; Billoud, B. *Chem. Rev.* **2007**, *107*, 4206–4272.
(2) Vincent, K. A.; Parkin, A.; Lenz, O.; Albracht, S. P. J.; Fontecilla-Camps, J. C.; Cammack, R.; Friedrich, B.; Armstrong, F. A. *J. Am. Chem. Soc.* **2005**, *127*, 18179–18189.
(3) Vincent, K. A.; Parkin, A.; Armstrong, F. A. *Chem. Rev.* **2007**, *107*, 4366–4413.
(4) Adams, M. W. W. *Biochim. Biophys. Acta* **1990**, *1020*, 115.
(5) Pierik, A. J.; Hagen, W. R.; Redeker, J. S.; Wolbert, R. B.; Boersma, M.; Verhagen, M. F.; Grande, H. J.; Veeger, C.; Mutsaers, P. H.; Sands, R. H. *Eur. J. Biochem.* **1992**, *209*, 63–72.
(6) Pereira, A. S.; Tavares, P.; Moura, I.; Moura, J. J. G.; Huynh, B. H. *J. Am. Chem. Soc.* **2001**, *123*, 2771–2782.
(7) Baffert, C.; Demuez, M.; Cournac, L.; Burlat, B.; Guigliarelli, B.; Bertrand, P.; Girbal, L.; Léger, C. *Angew. Chem., Int. Ed.* **2008**, *47*, 2052–2054.
(8) Buhrke, T.; Lenz, O.; Krauss, N.; Friedrich, B. *J. Biol. Chem.* **2005**, *280*, 23791–23796.
(9) Fan, H.-J.; Hall, M. B. *J. Am. Chem. Soc.* **2001**, *123*, 3828–3829.
(10) Cao, Z.; Hall, M. B. *J. Am. Chem. Soc.* **2001**, *123*, 3734–3742.
(11) Liu, Z.-P.; Hu, P. *J. Am. Chem. Soc.* **2002**, *124*, 5175–5182.
(12) Bruschi, M.; Fantucci, P.; De Gioia, L. *Inorg. Chem.* **2002**, *41*, 1421–1429.

Published on Web 07/06/2009

mechanisms of hydrogen oxidation/production[9−25] little is known so far about the molecular details leading to enzyme inactivation by dioxygen.[2,3,7,26]

Here, we present a theoretical investigation of the inhibition mechanism that uses density functional theory calculations on O_2 adducts of the active center of [FeFe]-hydrogenase. We demonstrate that the initial formation of a dioxygen bound form of the metal-cofactor is energetically favored and followed by irreversible reaction steps that can explain the experimentally observed dioxygen-induced enzyme inhibition.

2. Computational Methodology

All-electron calculations were carried out with the density functional theory (DFT) programs included in the Turbomole suite[27] on model structures of the active site of [FeFe]-hydrogenase taking the proximate Fe_4S_4 cluster explicitly into account (see Section 3, below). The models were treated as open-shell systems in the unrestricted Kohn−Sham framework. For the calculations, we used the Becke−Perdew exchange−correlation functional dubbed BP86[28,29] and the hybrid B3LYP functional.[30,31] For additional comparison purposes, we considered the recently developed TPSS functional.[32] For BP86 and TPSS we invoked the resolution-of-the-identity (RI) approximation as implemented in Turbomole. For all atoms included in our models, we used either the split-valence plus polarization functions (SVP) basis set[33] or Ahlrichs' valence triple-ζ TZVP basis set with polarization functions.[34] All molecular structures were fully optimized until the norm of the gradient had reached about 10^{-3} au, and the energetical difference of the last 20 structures in the optimization procedure was below 0.2 kcal/mol. The basis set superposition error of the TZVP basis set, with respect to coordination energies, amounts to about 2.4 kcal/mol[35] and should, therefore, not affect the analysis of dioxygen binding to the H-cluster. Hence, reaction energies have not been corrected for basis set superposition effects and were evaluated at 0 K without vibrational and temperature corrections. Protonation energies were calculated by assuming for a solvated proton an energy of −262.4 kcal/mol.[36,37] Local spin analyses, according to Mulliken and Löwdin decomposition schemes, have been performed with our local version of the Moloch module of Turbomole.[38,39] Images of molecular structures were created with Pymol.[40]

3. Details of the Molecular System under Study

In this study, we focus on the H-cluster of [FeFe]-hydrogenase whose molecular architecture has been revealed by X-ray crystallography.[41−43] It consists of a special 2-Fe center — the $[2Fe]_H$ subcluster — that is considered to carry the catalytic activity. It is linked by the sulfur atom of a cysteine residue to a $[Fe_4S_4]$ cubane (Figure 1b). With respect to their distance from the $[Fe_4S_4]$ component, the iron atoms of the $[2Fe]_H$ subsite are referred to as proximal (Fe_p) and distal (Fe_d) iron centers (Figure 1b). The $[2Fe]_H$ cluster is coordinated by ligands unusual in living systems like CN^- and CO and a dithiolate-moiety that μ-bridges both iron atoms. A Lewis structure of the H-cluster can be seen in Figure 2.

The active site is embedded in the protein interior (Figure 1a) and connected to the environment via a gas diffusion and a proton channel.[42] A species dependent number of accessory $[Fe_4S_4]$ clusters is considered to facilitate electron transfer from donor molecules such as ferredoxin to the H-cluster.[41,42] All calculations discussed here are based on the H-cluster from the 1.4 Å crystal structure of [FeFe]-hydrogenase from *Clostridium pasteurianum* (PDB entry 3C8Y).[43]

Different redox states of the H-cluster have been characterized experimentally. It is believed that two of them are relevant for the catalytic cycle of the enzyme—one EPR-active, oxidized form (H_{ox}^{cat}) and a reduced one (H_{red}^{cat}), which is EPR-silent.[19,44] Further oxidation of H_{ox}^{cat} yields an inactive species (H_{ox}^{inact}) that can be reactivated under reducing conditions.[2,3]

The assignment of redox states to the available experimental structures of the H-cluster is a matter of controversy. The crystal structure used in the present computational study was solved from a protein sample obtained under anaerobic condidtions, and therefore, it is likely that it corresponds

(13) Bruschi, M.; Fantucci, P.; De Gioia, L. *Inorg. Chem.* **2003**, *42*, 4773–4781.
(14) Bruschi, M.; Fantucci, P.; De Gioia, L. *Inorg. Chem.* **2004**, *43*, 3733–3741.
(15) Zhou, T.; Mo, Y.; Liu, A.; Zhou, Z.; Tsai, K. R. *Inorg. Chem.* **2004**, *43*, 923–930.
(16) Tye, J. W.; Lee, J.; Wang, H.-W.; Mejia-Rodriguez, R.; Reibenspies, J. H.; Hall, M. B.; Darensbourg, M. Y. *Inorg. Chem.* **2005**, *44*, 5550–5552.
(17) Zampella, G.; Bruschi, M.; Fantucci, P.; Gioia, L. D. *J. Am. Chem. Soc.* **2005**, *127*, 13180–13189.
(18) Tye, J. W.; Darensbourg, M. Y.; Hall, M. B. *J. Comput. Chem.* **2006**, *27*, 1454–1462.
(19) Greco, C.; Bruschi, M.; De Gioia, L.; Ryde, U. *Inorg. Chem.* **2007**, *46*, 5911–5921.
(20) Siegbahn, P. E. M.; Tye, J. W.; Hall, M. B. *Chem. Rev.* **2007**, *107*, 4414–4435.
(21) Borg, S. J.; Tye, J. W.; Hall, M. B.; Best, S. P. *Inorg. Chem.* **2007**, *46*, 384–394.
(22) Thomas, C. M.; Darensbourg, M. Y.; Hall, M. B. *J. Inorg. Biochem.* **2007**, *101*, 1752–1757.
(23) Tye, J. W.; Darensbourg, M. Y.; Hall, M. B. *Inorg. Chem.* **2008**, *47*, 2380–2388.
(24) Thomas, C. M.; Liu, T.; Hall, M. B.; Darensbourg, M. Y. *Inorg. Chem.* **2008**, *47*, 7009–7024.
(25) Yang, X.; Hall, M. B. *J. Am. Chem. Soc.* **2008**, *130*, 14036–14037.
(26) Dogaru, D.; Motiu, S.; Gogonea, V. *Int. J. Quantum Chem.* **2009**, *109*, 876–889.
(27) Ahlrichs, R.; Bär, M.; Häser, M.; Horn, H.; Kölmel, C. *Chem. Phys. Lett.* **1989**, *162*, 165–169.
(28) Becke, A. D. *Phys. Rev. A: At., Mol., Opt. Phys.* **1988**, *38*, 3098–3100.
(29) Perdew, J. W. *Phys. Rev. B: Condens. Matter Mater. Phys.* **1986**, *33*, 8822–8824.
(30) Lee, C.; Yang, W.; Parr, R. G. *Phys. Rev. B: Condens. Matter Mater. Phys.* **1988**, *37*, 785–789.
(31) Becke, A. D. *J. Chem. Phys.* **1993**, *98*, 5648–5652.
(32) Tao, J.; Perdew, J. P.; Staroverov, V. N.; Scuseria, G. E. *Phys. Rev. Lett.* **2003**, *91*, 146401.
(33) Schäfer, A.; Horn, H.; Ahlrichs, R. *J. Chem. Phys.* **1992**, *97*, 2571–2577.
(34) Schäfer, A.; Huber, C.; Ahlrichs, R. *J. Chem. Phys.* **1994**, *100*, 5829−5835.
(35) Reiher, M.; Hess, B. A. *Chem.−Eur. J.* **2002**, *8*, 5332–5339.
(36) Klots, C. E. *J. Phys. Chem.* **1981**, *85*, 3585–3588.
(37) Topol, I. A.; Tawa, G. J.; Burt, S. K.; Rashin, A. A. *J. Phys. Chem.* **1997**, *101*, 10075–10081.
(38) Herrmann, C.; Reiher, M.; Hess, B. A. *J. Chem. Phys.* **2005**, *122*, 034102.
(39) Podewitz, M.; Herrmann, C.; Malassa, A.; Westerhausen, M.; Reiher, M. *Chem. Phys. Lett.* **2008**, *451*, 301–308.
(40) DeLano, W. L. *The PyMOL Molecular Graphics System*; DeLano Scientific: San Carlos, CA, 2002.
(41) Peters, J. W.; Lanzilotta, W. N.; Lemon, B. J.; Seefeldt, L. C. *Science* **1998**, *282*, 1853–1858.
(42) Nicolet, Y.; Piras, C.; Legrand, P.; Hatchikian, C. E.; Fontecilla-Camps, J. C. *Structure* **1999**, *7*, 13–23.
(43) Pandey, A. S.; Harris, T. V.; Giles, L. J.; Peters, J. W.; Szilagyi, R. K. *J. Am. Chem. Soc.* **2008**, *130*, 4533–4540.
(44) Lubitz, W.; Reijerse, E.; van Gastel, M. *Chem. Rev.* **2007**, *107*, 4331–4365.

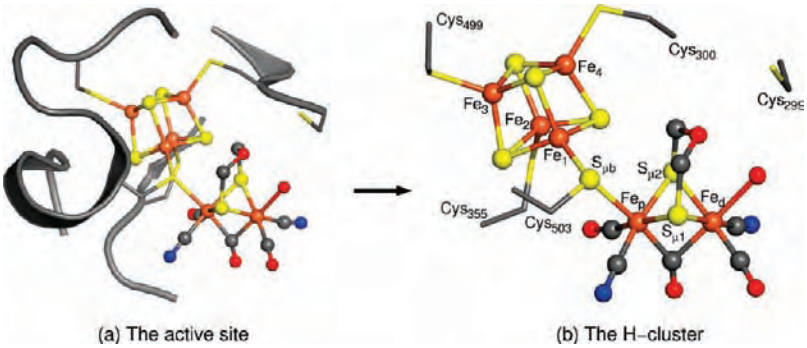

Figure 1. [FeFe]-hydrogenase. A look at the active site and the isolated H-cluster of [FeFe]-hydrogenase from *Clostridium pasteurianum* (PDB entry 3C8Y). The same nomenclature of the atoms is used throughout the text. Element color code — red: O, gray: C, blue: N, yellow: S, and brown: Fe.

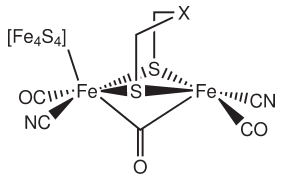

Figure 2. Lewis structure of the H-cluster of [FeFe]-hydrogenase. For the bridge-headgroup X, two possibilities are considered: X = O and X = NH.

to the oxidized active $[Fe_p(I)Fe_d(II)]$ form of the active site as proposed by Pandey et al.[43] In this configuration the cluster is EPR-active and was shown to be in a doublet state.[19,44] However, the fact that the structure contains an oxygen atom attached to Fe_d (Figure 1a) that, most certainly belongs to a water molecule,[43] could also imply an EPR-silent $[Fe_p(II)Fe_d(II)]$ pair as suggested by theoretical studies on the catalytic cycle of the enzyme from *Desulfovibrio desulfuricans*.[19]

It was shown that in both states H_{ox}^{cat} and H_{red}^{cat} the $[Fe_4S_4]$ cluster is EPR-silent and can formally be considered as having an oxidation state of +II.[6,44,45] In this study, we consider the cubane as a formally double-positively charged moiety $[Fe_4S_4]$ combined with the formally negatively charged $[2Fe]_H$ subsite denoted as a $[Fe_p(II)Fe_d(II)]$ pair in the case of H_{ox}^{inact} and as a $[Fe_p(I)Fe_d(II)]$ pair in the case of H_{ox}^{cat} to yield a total charge of −2 for H_{ox}^{inact} and −3 for H_{ox}^{cat}, respectively. Note that the cluster-anchoring cysteine residues also contribute negative charges which need to be taken into account for the calculation of the net charge. The cyanide and the bridging dithiolate ligands are considered to contribute a charge of −1 and −2, respectively.

In addition to both metal clusters, our models contain the three cysteine residues Cys_{300}, Cys_{355}, and Cys_{499} with which the $[Fe_4S_4]$ cluster is anchored within the protein and the subcluster-bridging cysteine Cys_{503} (Figure 1b). Furthermore, we include Cys_{300} that is located in close proximity to the distal Fe_d, and which is considered to be involved in proton transport.[41] All but one cysteine residues were modeled as thiomethanolate moieties with spatially fixed methyl groups. The remaining cysteine is spatially fixed via its methyl group and carries a hydrogen atom but does not coordinate to an iron center and, thus, does not anchor the cluster. All other atoms were not subjected to any restraints during structure optimiziations.

4. Structural Validation

In order to validate our computational approach, we aimed at reproducing the crystal structure of the H-cluster using different functionals and basis sets. We included an oxygen atom, which in PDB entry 3C8Y, is located next to Fe_d as a water molecule in our starting model and considered both the H_{ox}^{inact} form, which corresponds formally to $[Fe_4S_4][Fe_p(II)Fe_d(II)]$, and the H_{ox}^{cat} form that can be described as a $[Fe_4S_4][Fe_p(I)Fe_d(II)]$ configuration. The overall charge of the model is −2 elementary charges for H_{ox}^{inact} and will be referred to as $\mathbf{1}$−$[Fe_p(II)Fe_d(II)]^{2-}$ with an oxygen atom as the bridge-head atom at the dithiolate ligand and as $\mathbf{1(NH)}$−$[Fe_p(II)Fe_d(II)]^{2-}$ with an NH group, correspondingly. Similarly, the charge of the H_{ox}^{cat} model is − 3 elementary charges, and the two compounds will be denoted as $\mathbf{1}$−$[Fe_p(I)Fe_d(II)]^{3-}$ and $\mathbf{1(NH)}$−$[Fe_p(I)Fe_d(II)]^{3-}$, respectively. We will use a similar naming convention for all considered species throughout the whole manuscript, but note that the assignment of oxidation numbers to the iron atoms is used here mainly for labeling purposes and have to be considered with care. Especially the assignment of high oxidation numbers must not be taken too literally.

In addition to the functionals BP86 and B3LYP, we also consider the TPSS functional for our calculations to obtain a better overview of the structural deviations to be expected when studying reaction pathways of [FeFe]-hydrogenase by means of approximate density functionals. Naturally, the approximate nature of contemporary density functionals, which cannot be improved in a systematical manner, sets limitations to the accuracy. We are advised to study the scatter of calculated data in order to assess the validity of our conclusions and to check on internal consistency.

Interestingly, Table 1 and Figure 3 show that all functionals considered describe characteristic interatomic distances of the H-cluster reasonably well and give similar results. Some deviations from the crystal structure can be seen for the overall orientation of the $[2Fe]_H$ subsite with respect to the $[Fe_4S_4]$ cluster, which are more pronounced for the B3LYP functional (Figure 3d).

The same calculations performed by assuming an overall charge of the H-cluster of −3 elementary charges—which corresponds to the oxidized, active form H_{ox}^{cat}—revealed a significantly increased distance between Fe_d and the attached water molecule (> 3.5 Å, see Figure 4 and Table 2). Other

(45) Popescu, C. V.; Münck, E. *J. Am. Chem. Soc.* **1999**, *121*, 7877–7884.

Table 1. Structural Features of the DFT-Optimized H-Clusters Shown in Figure 3[a]

		1−[Fe_p(II)Fe_d(II)]$^{2-}$			**1**(**NH**)−[[Fe_p(II)Fe_d(II)]$^{2-}$		
	exp.	BP86	B3LYP	TPSS	BP86	B3LYP	TPSS
				Distances			
$Fe_p\cdots Fe_d$	2.55	2.55	2.59	2.55	2.55	2.59	2.55
$Fe_d\cdots O(H_2O)$	2.38	3.50	3.89	3.42	3.89	3.69	3.59
$Fe_p\cdots S_{\mu_1}$	2.29	2.37	2.41	2.37	2.39	2.41	2.37
$Fe_p\cdots S_{\mu_2}$	2.30	2.34	2.37	2.34	2.31	2.38	2.33
$Fe_p\cdots C(O)$	1.74	1.75	1.79	1.76	1.76	1.78	1.77
$Fe_p\cdots C(N)$	1.83	1.92	1.95	1.93	1.92	1.96	1.93
$Fe_d\cdots S_{\mu_1}$	2.32	2.31	2.36	2.31	2.32	2.35	2.31
$Fe_d\cdots S_{\mu_2}$	2.30	2.34	2.37	2.34	2.31	2.37	2.33
$Fe_d\cdots C(O)$	1.77	1.75	1.78	1.76	1.75	1.78	1.76
$Fe_d\cdots C(N)$	1.93	1.92	1.96	1.93	1.92	1.96	1.93
$Fe_p\cdots S_{\mu_b}$	2.39	2.43	2.42	2.43	2.42	2.42	2.40
$Fe_p\cdots C(CO_\mu)$	1.91	1.99	2.11	2.01	1.96	2.12	2.01
$Fe_d\cdots C(CO_\mu)$	1.99	1.91	1.91	1.91	1.92	1.90	1.91
				Angles			
$Fe_p-S_{\mu_b}-Fe_1$	117.1	122.7	125.4	122.2	127.9	127.2	124.3
$Fe_4-Fe_1-S_{\mu_b}-Fe_p$	−87.4	−79.8	−79.2	−81.2	−68.6	−69.4	−74.5

[a] For all optimizations, the TZVP basis set was used. The charge of the cluster is −2 elementary charges in each case, corresponding to a [Fe_p(II)Fe_d(II)]-pair at the $[2Fe]_H$ subsite.

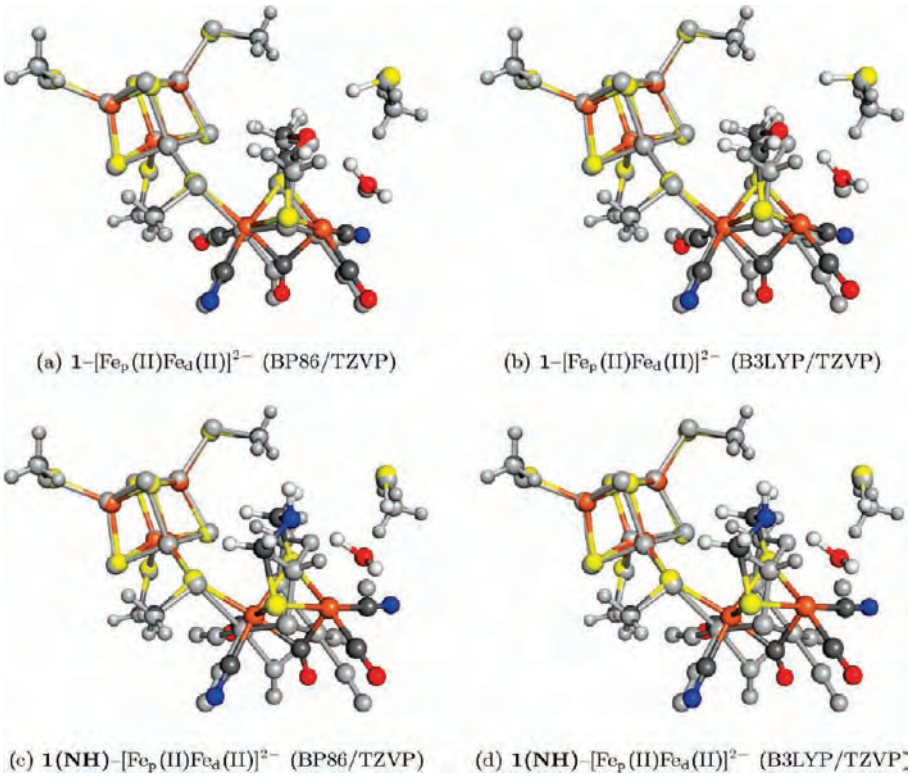

Figure 3. Superpositions of DFT-optimized structures (BP86 left, B3LYP right) with the coordinates obtained from the crystal structure (gray) of PDB entry 3C8Y.[43] *Upper panel*: Bridging atom O. *Lower panel*: Bridging group NH.

bond distances are not severely affected by a change in the overall charge, and it is, therefore, not possible to assign the redox state of the system unambiguously based on the calculations.

An ongoing discussion addresses the identity of the bridgehead atom of the dithiolate ligand that connects the two Fe-atoms of the $[2Fe]_H$ subsite. In a recent publication, Pandey et al. compared several possibilities and proposed an oxygen atom at this position.[43] We considered two variants: oxygen and singly protonated nitrogen, as proposed by different groups.[41,42,46] Using DFT calculations, Fan and Hall showed that NH as bridge-headgroup can act as a suitable base in the catalytic cycle of the enzyme.[9] Based on the optimized structures, one can see that the characteristic distances do

(46) Nicolet, Y.; de Lacey, A. L.; Vernde, X.; Fernandez, V. M.; Hatchikian, E. C.; Fontecilla-Camps, J. C. *J. Am. Chem. Soc.* **2001**, *123*, 1596–1601.

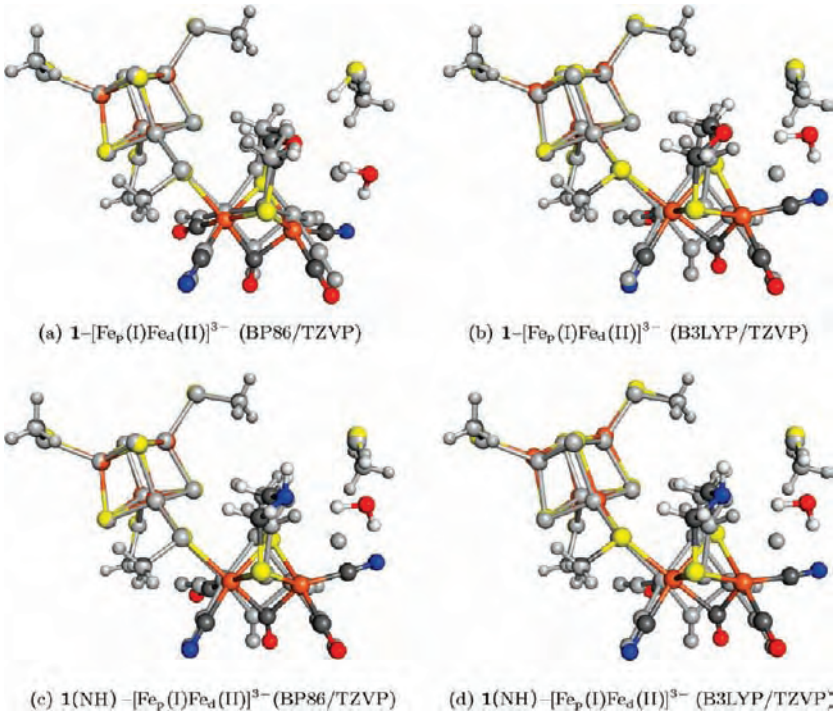

Figure 4. Superpositions of DFT-optimized structures (BP86 left, B3LYP right) with the coordinates obtained from the crystal structure (gray) of PDB entry 3C8Y.[43] *Upper panel*: Bridging atom O. *Lower panel*: Bridging group NH.

Table 2. Structural Features of the DFT-Optimized H-Clusters Shown in Figure 4[a]

		1–[Fe$_p$(I)Fe$_d$(II)]$^{3-}$			**1(NH)**–[[Fe$_p$(I)Fe$_d$(II)]$^{3-}$		
	exp.	BP86	B3LYP	TPSS	BP86	B3LYP	TPSS
			Distances				
Fe$_p$···Fe$_d$	2.55	2.55	2.59	2.55	2.55	2.59	2.55
Fe$_d$···O(H$_2$O)	2.38	3.50	3.89	3.42	3.89	3.69	3.59
Fe$_p$···S$_{\mu_1}$	2.29	2.37	2.41	2.37	2.39	2.41	2.37
Fe$_p$···S$_{\mu_2}$	2.30	2.34	2.37	2.34	2.31	2.38	2.33
Fe$_p$···C(O)	1.74	1.75	1.79	1.76	1.76	1.78	1.77
Fe$_p$···C(N)	1.83	1.92	1.95	1.93	1.92	1.96	1.93
Fe$_d$···S$_{\mu_1}$	2.32	2.31	2.36	2.31	2.32	2.35	2.31
Fe$_d$···S$_{\mu_2}$	2.30	2.34	2.37	2.34	2.31	2.37	2.33
Fe$_d$···C(O)	1.77	1.75	1.78	1.76	1.75	1.78	1.76
Fe$_d$···C(N)	1.93	1.92	1.96	1.93	1.92	1.96	1.93
Fe$_p$···S$_{\mu_b}$	2.39	2.43	2.42	2.43	2.42	2.42	2.40
Fe$_p$···C(CO$_\mu$)	1.91	1.99	2.11	2.01	1.96	2.12	2.01
			Angles				
Fe$_p$–S$_{\mu_b}$–Fe$_1$	117.1	126.5	128.0	124.8	130.3	129.2	130.9
Fe$_4$–Fe$_1$–S$_{\mu_b}$–Fe$_p$	−87.4	−87.0	−80.9	−89.7	−79.3	−83.9	−77.4
Fe$_d$···C(CO$_\mu$)	1.99	1.91	1.91	1.91	1.92	1.90	1.91

[a] For all optimizations, the TZVP basis set was used. The charge of the cluster is −3 elementary charges in each case, corresponding to a [Fe$_p$(I)Fe$_d$(II)]-pair at the [2Fe]$_H$ subsite.

not change significantly upon substitution of oxygen by a NH-group (Figures 3 and 4, Tables 1 and 2). However, the reorientation of the [2Fe]$_H$ subsite, with respect to the [Fe$_4$-S$_4$] cluster, is much more pronounced in this case, especially for the oxidized active form of the enzyme. In this study, we focus, therefore, on the oxygen variant of the dithiolate ligand in line with the experimental and computational results of ref 43 and with the assignment in the corresponding PDB entry 3C8Y[43] (see also Section 6 for discussion of the reaction energies for oxygen addition to the cluster).

5. Spin Coupling in the Active Form of [FeFe]-Hydrogenase

Because of the involvement of six iron atoms in the H-cluster, the spin coupling schemes can be very intricate. It is thought that the [Fe$_4$S$_4$] cluster consists of two Fe$_2$S$_2$ layers in a high spin state that couple antiferromagnetically to give a formally diamagnetic state.[47,48]

(47) Fiedler, A. T.; Brunold, T. C. *Inorg. Chem.* **2005**, *44*, 9322–9334.
(48) Bruschi, M.; Greco, C.; Fantucci, P.; De Gioia, L. *Inorg. Chem.* **2008**, *47*, 6056–6071.

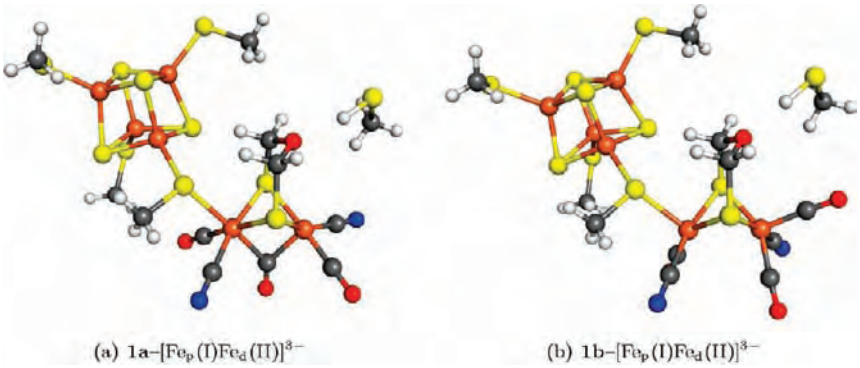

Figure 5. Optimized structures (BP86/TZVP) of the bridged and the terminal CO isomer of the active form H_{ox}^{cat} of [FeFe]-hydrogenase.

Table 3. $\langle S_{zFe} \rangle$ Expectation Values in Atomic Units for the Two CO Isomers **1a,b** –[Fe$_p$(I)Fe$_d$(II)]$^{3-}$ of the H-Cluster of [FeFe]-Hydrogenase[a]

	local spins $\langle S_{zFe} \rangle$		Mulliken charges	
	1a	**1b**	**1a**	**1b**
Fe$_d$	0.41	−0.02	−0.50	−0.64
Fe$_p$	0.05	0.48	−0.66	−0.53
Fe$_1$	−1.49	−1.54	−0.33	−0.29
Fe$_2$	1.48	−1.51	−0.32	−0.31
Fe$_3$	−1.50	1.55	−0.32	−0.28
Fe$_4$	1.51	1.51	−0.32	−0.32

[a] These expectation values correspond to half of the α- and β-spin populations at the Fe atoms and refer to structures optimized with BP86/TZVP as depicted in Figure 5. Partial charges derived from Mulliken population analysis in atomic units are also given.

Since we are interested in the inactivation of [FeFe]-hydrogenase by dioxygen, we start with the active form H_{ox}^{cat} to which a redox state [Fe$_4$S$_4$][Fe$_p$(I)Fe$_d$(II)] can be assigned, corresponding to an overall charge of −3 elementary charges as mentioned above (the [Fe$_4$S$_4$] subcluster is then considered to carry +2 elementary charges). With respect to the orientation of the CO ligands, two different isomers of the [2Fe]$_H$ subcluster are possible — the arrangement, as it is present in the crystal structure, with one CO bridging Fe$_p$ and Fe$_d$ referred to as **1a**–[Fe$_p$(I)Fe$_d$(II)]$^{3-}$ (Figure 5a) and a terminal isomer in which the CO ligand points toward the other direction at the distal Fe (Figure 5b), which we call **1b**–[Fe$_p$-(I)Fe$_d$(II)]$^{3-}$ in the following.

Both structures were optimized with BP86/TZVP and B3LYP/TZYP, and the spin couplings were determined by population analysis (Table 3).[38] With a $\langle S^2 \rangle$ expectation value of approximately 7.4 atomic units (i.e., in units where the rest mass of the electron, its absolute charge, and the reduced Planck constant take values of 1), the DFT wave functions of both isomers show a high degree of spin contamination as is usually to be expected in the case of broken-symmetry determinants for such clusters. For the terminal isomer **1b**–[Fe$_p$(I)Fe$_d$(II)]$^{3-}$ (Figure 5b), we arrive at the same coupling scheme as presented in ref 48 in which the pair Fe$_1$–Fe$_2$ of the [Fe$_4$S$_4$] cubane couples antiferromagnetically with the pair Fe$_3$–Fe$_4$ and the spin localized at Fe$_p$ (Table 3, numbering as in Figure 1b). A different solution is obtained, however, for the bridged isomer **1a**–[Fe$_p$(I)Fe$_d$(II)]$^{3-}$ (Figure 5a). The antiferromagnetic coupling now occurs between Fe$_1$–Fe$_3$ and Fe$_2$–Fe$_4$. According to the results in ref 48, the spin of the [2Fe]$_H$ subsite is located at Fe$_d$ and couples antiferromagnetically with Fe$_1$. In order to analyze the discrepancies regarding the [Fe$_4$S$_4$] cluster, we recalculated the molecular wave function of **1a**–[Fe$_p$(I)Fe$_d$(II)]$^{3-}$ with the coupling obtained for isomer **1b**–[Fe$_p$(I)Fe$_d$(II)]$^{3-}$ by starting from the converged orbitals of the terminal isomer. The different coupling scheme resulted in a slightly higher energy (+5.1 kcal/mol, BP86/TZVP). However, one must note that this value is the result of a single-point calculation and the system can relax to a state of lower energy. After geometry optimization, the resulting structure was only −1.3 kcal/mol more stable than that of the system described by the $\langle S_{zFe} \rangle$ values given in Table 3, which is the reason why we consider energetic differences due to alternative spin coupling to be negligible for the validity of our results regarding dioxygen addition to the H-cluster. We, therefore, employed the standard DFT geometry optimization approach for our calculations without using explicit spin localization procedures[49] and always accepted the spin density distribution calculated by the Turbomole program. Note also that it was shown that the geometry of the [2Fe]$_H$ subsite is not strongly affected by the presence of the [Fe$_4$S$_4$] cluster.[48] In addition to the local spin data, Table 3 provides Mulliken partial charges for all iron centers, which turn out to all feature negative partial charges. As can be seen from the table, the partial charges of the two isomers differ slightly. These differences, however, should not be considered further in view of the conceptual problem of assigning partial charges in general and Mulliken charges in particular.

6. Reaction Pathways with Dioxygen

In this section as well as in the following section 7, we present reaction energies for possible O_2-addition pathways with subsequent protonation and reduction steps, as calculated from electronic energy differences. Because of the large number of possible reaction sites and products, an overview is given in Figure 7.

Depending on the ligand arrangement discussed above, dioxygen can, in principle, attack the active form of the H-cluster along two different pathways. For the bridged isomer, as it is found in the crystal structure, O_2 can approach most easily the distal iron atom Fe$_d$ (Figure 6a). This isomer is abbreviated as **2a**–[Fe$_p$(II)Fe$_d$(II)]$^{3-}$ in the following. In the case of the terminal conformation, there are two orientations for the oxygen molecule in order to complete an octahedral ligand sphere at Fe$_p$ and Fe$_d$—one where the

(49) Herrmann, C.; Podewitz, M.; Reiher, M. *Int. J. Quantum Chem.* **2009**, *109*, 2430–2446.

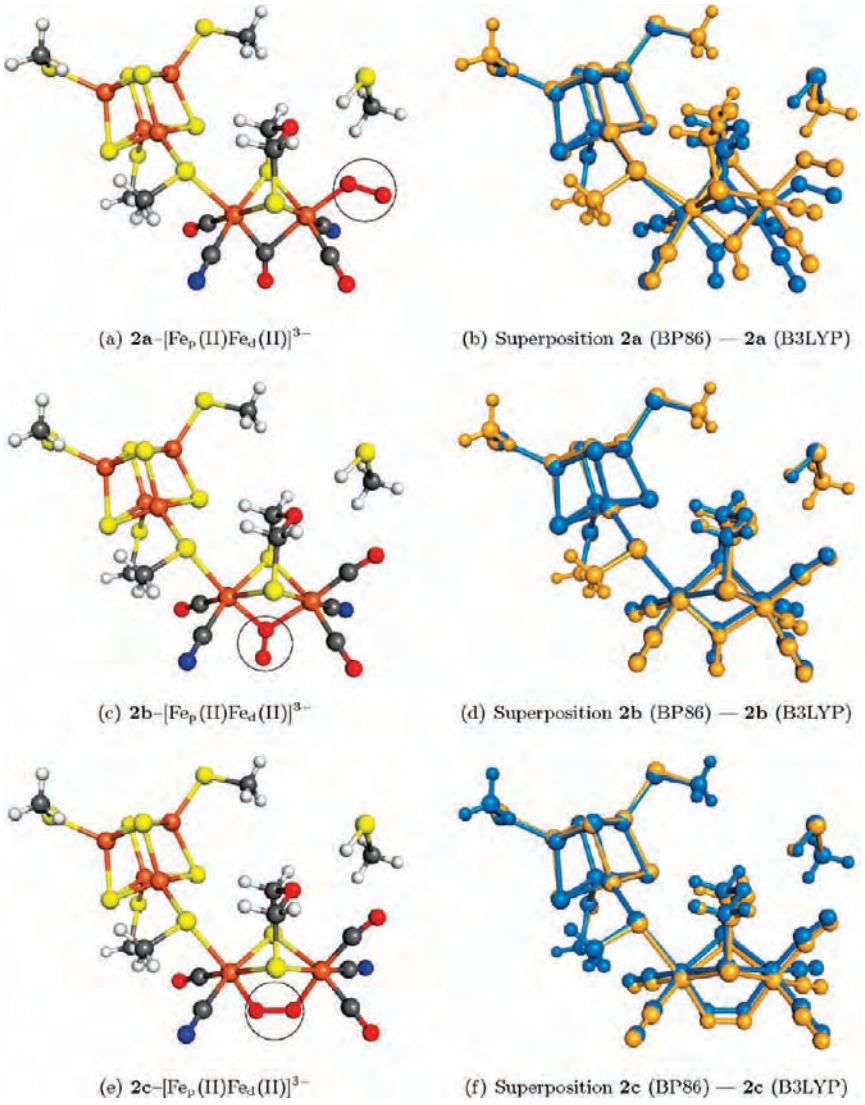

Figure 6. Dioxygen adducts of [FeFe]-hydrogenase. *Left panel*: Structures of three different O_2 adducts of [FeFe]-hydrogenase optimized with BP86/TZVP. The oxygen molecule is highlighted by a black circle. *Right panel*: Superpositions of these structures (blue) with B3LYP/TZVP optimized structures (orange).

whole O_2 molecule bridges both iron atoms and a second form in which only one oxygen atom is directly involved in a bridge (Figures 6c and 6e). These two isomers are referred to as **2b**–[Fe$_p$(II)Fe$_d$(II)]$^{3-}$ and **2c**–[Fe$_p$(II)Fe$_d$(II)]$^{3-}$, respectively.

DFT-optimized structures of the three O_2 adducts are shown in Figure 6. In order to estimate whether the addition of dioxygen is energetically favored for any of these possibilities, reaction energies were calculated from the energies of the oxygen-free cluster **1a**–[Fe$_p$(I)Fe$_d$(II)]$^{3-}$, the dioxygen adducts, and triplet O_2. Table 4 shows that the reaction energies obtained with different combinations of density functionals/basis sets scatter over a relatively large range. While the TZVP basis set always gives more reliable data than the smaller SVP basis set, all differences between TZVP data obtained with different functionals must be attributed to the approximations made in the construction of the functionals. For the BP86 functional, the terminal O_2 adduct is the most stable form independent of the basis set applied. The corresponding reaction should, therefore, be exothermic. A very similar reaction energy (−67.1 kcal/mol) results with the TPSS functional and the TZVP basis set, so we chose to concentrate on the BP86 functional for further discussion. It is important to note that the identity of the bridge-head atom of the dithiolate ligand does not affect this reaction energy significantly. Structure optimization, after replacing the oxygen atom by an NH group, yields a value of −71.7 kcal/mol (BP86/TZVP), which is similar to that obtained for the oxygen-variant (64.5 kcal/mol). Our conclusions should, therefore, be valid irrespective of the chemical nature of the bridge-headgroup.

The result for the terminal O_2 adduct **2a**–[Fe$_p$(II)Fe$_d$(II)]$^{3-}$ is corroborated by calculations performed with B3LYP and the larger TZVP basis set. With the SVP basis set, however, O_2 adduct **2c**–[Fe$_p$(II)Fe$_d$(II)]$^{3-}$ is predicted to be the most stable isomer, which, thus, must be an artifact of the smaller basis set, as the TZVP basis set is clearly more reliable. This severe discrepancy demonstrates that, especially for the B3LYP functional, it is important to use a large basis set in order to describe the energetics of hydrogenase adequately and that small double-ζ basis sets should not be used. Despite the large variations between the reaction

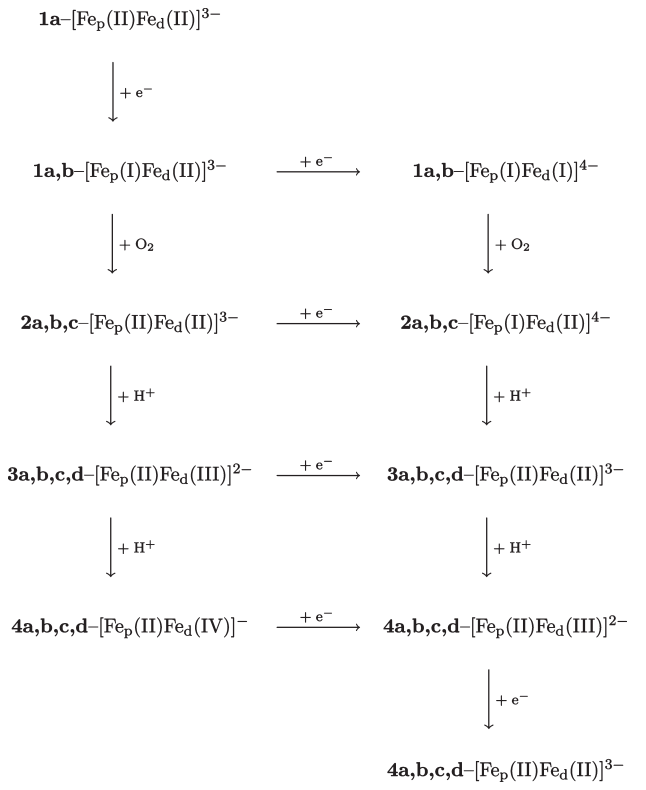

Figure 7. Overview of possible O_2-inhibition pathways for [FeFe]-hydrogenase, as discussed in Sections 6 and 7. The scheme shows the nomenclature for all species and isomers considered.

Table 4. Reaction Energies for the Formation of the O_2-Adducts **2a,b,c**–[Fe$_p$(II)Fe$_d$(II)]$^{3-}$ of [FeFe]-hydrogenase shown in Figure 6[a]

	2a	2b	2c
Geometry Optimization			
BP86/SVP	−78.8	−7.2	−23.6
BP86/TZVP	−64.5	−13.3	−17.1
B3LYP/SVP	−10.1	−0.8	−24.2
B3LYP/TZVP	−40.3	−8.7	−5.5
Cross Calculations at Single-Points			
BP86/TZVP//B3LYP/TZVP	−61.2	−4.4	−22.6
B3LYP/TZVP//BP86/TZVP	−65.0	−46.0	−58.2

[a] Energies are given in kcal/mol.

energies obtained with BP86 and B3LYP, it is clear that the terminal O_2 adduct **2a**–[Fe$_p$(II)Fe$_d$(II)]$^{3-}$ is energetically favored and should be the preferred reaction product. The O–O bond length of 1.31 Å, given in Table 5, lies between experimental values for the superoxide ion in KO_2 (1.28 Å)[50] and in the solid phase (1.33 Å)[51] and compares well with a range of 1.32–1.35 Å determined for hemoproteins[52,53] by DFT calculations, where the iron–dioxygen-adduct is alternatively described as a ferric-peroxo or a ferrous-superoxo species. This means that, upon interaction with dioxygen, the

(50) Abrahams, S. C.; Kalnajs, J. *Acta Crystallogr.* **1955**, *8*, 503–506.
(51) Dietzel, P. D. C.; Kremer, R. K.; Jansen, M. *J. Am. Chem. Soc.* **2004**, *126*, 4689–4696.
(52) Silaghi-Dumitrescu, R.; Cooper, C. E. *Dalton Trans.* **2005**, 3477–3482.
(53) Harris, D.; Loew, G.; Waskell, L. *J. Am. Chem. Soc.* **1998**, *120*, 4308.

Table 5. O–O Bond Lengths in the Different O_2-Adducts in Å[a]

	O–O bond length
Oxygen Adducts	
2a–[Fe$_p$(II)Fe$_d$(II)]$^{3-}$	1.31/1.31
2b–[Fe$_p$(II)Fe$_d$(II)]$^{3-}$	1.32/1.31
2c–[Fe$_p$(II)Fe$_d$(II)]$^{3-}$	1.37/1.33
Singly Protonated Species	
3a–[Fe$_p$(II)Fe$_d$(III)]$^{2-}$	1.46
3b–[Fe$_p$(II)Fe$_d$(III)]$^{2-}$	1.48
3c–[Fe$_p$(II)Fe$_d$(III)]$^{2-}$	1.78
3d–[Fe$_p$(II)Fe$_d$(III)]$^{2-}$	1.51

[a] In each row, the first number refers to structures optimized with BP86/TZVP and the second number to B3LYP/TZVP (where available).

Table 6. Local $\langle S_{zA} \rangle$ Expectation Values (top) and Mulliken Partial Charges (bottom) in Atomic Units for the O_2-Adducts **2a,b,c**–[Fe$_p$(II)Fe$_d$(II)]$^{3-}$ of [FeFe]-hydrogenase (shown in Figure 6) and the Protonated Forms **3a,b,c**–[Fe$_p$(II)Fe$_d$(II)]$^{3-}$ and **4a**–[Fe$_p$(II)Fe$_d$(II)]$^{3-}$ (shown in Figure 8)[a]

A	2a	2b	2c	3a	3b	3c	4a
Local Spins $\langle S_{zA} \rangle$							
O$_p$	−0.22	0.17	−0.18	0.07	0.01	0.09	0.03
O$_d$	−0.25	0.23	−0.13	0.02	0.00	−0.03	0.00[b]
Fe$_d$	−0.02	−0.06	−0.01	0.09	0.00	−0.01	−0.07
Fe$_p$	0.03	−0.09	−0.18	0.01	0.17	0.25	−0.01
Fe$_1$	1.50	−1.55	1.53	1.47	1.49	−1.42	−1.28
Fe$_2$	−0.87	−1.51	−0.89	−1.30	−1.32	−1.41	1.39
Fe$_3$	−1.28	1.54	−1.28	−1.35	−1.33	1.50	1.43
Fe$_4$	1.48	1.51	1.50	1.45	1.46	1.46	−1.11
Mulliken Partial Charges							
O$_p$	−0.01	−0.06	−0.04	−0.16	−0.04	−0.11	−0.18
O$_d$	−0.24	−0.23	−0.13	−0.21	−0.20	−0.18	−0.45[b]
Fe$_d$	−0.55	−0.58	−0.56	−0.51	−0.59	−0.56	−0.41
Fe$_p$	−0.67	−0.58	−0.57	−0.69	−0.56	−0.54	−0.71
Fe$_1$	−0.31	−0.29	−0.29	−0.33	−0.32	−0.34	−0.38
Fe$_2$	−0.48	−0.30	−0.47	−0.37	−0.36	−0.34	−0.34
Fe$_3$	−0.38	−0.28	−0.38	−0.35	−0.37	−0.30	−0.33
Fe$_4$	−0.34	−0.32	−0.33	−0.37	−0.36	−0.34	−0.46

[a] Values refer to structures optimized with BP86/TZVP. O$_d$ refers to the oxygen atom of O_2 that binds directly to Fe$_d$, and O$_p$ denotes the oxygen atom that either binds to Fe$_p$ or that is free depending on the isomer considered. [b] For isomer **4a** atom, O$_p$ belongs to the released water molecule.

H-cluster is oxidized by one electron. In terms of formal oxidation states, the $[2Fe]_H$ subsite could correspond to either a [Fe$_p$(I)Fe$_d$(III)] or a [Fe$_p$(II)Fe$_d$(II)] pair. As can be seen from the $\langle S_{zA} \rangle$ expectation values in Table 6, the spin of the $[2Fe]_H$ is distributed on both oxygen atoms. For the sake of completeness, Table 6 also lists the Mulliken partial charges. As already noted in the case of **1a** and **1b**, the partial charges on all iron centers are negative and vary slightly between the different clusters. The same holds true for the oxygen atoms. As before, these slight differences in partial charge between the atoms of the different model clusters must not be overinterpreted.

In order to analyze differences in reaction energies in more detail, we cross-validated the data by single-point calculations with the functionals BP86 and B3LYP on the structures optimized with the respective other functional. Table 4 shows that for adduct **2a**–[Fe$_p$(II)Fe$_d$(II)]$^{3-}$, the

Table 7. Structural features of the DFT-optimized O_2 adducts **2a,b,c**−$[Fe_p(II)Fe_d(II)]^{3-}$ depicted in Figure 6[a]

	2a		2b		2c	
	BP86	B3LYP	BP86	B3LYP	BP86	B3LYP
			distances			
$Fe_d\cdots O(O_2)$	1.92	1.93	—	—	—	—
$Fe_p\cdots C(CO)$	—	—	1.75	1.79	1.76	1.80
$Fe_p\cdots Fe_d$	2.61	2.64	3.04	3.06	3.30	3.30
$Fe_p\cdots S_{\mu_1}$	2.37	2.39	2.43	2.46	2.39	2.42
$Fe_p\cdots S_{\mu_2}$	2.33	2.36	2.39	2.43	2.37	2.42
$Fe_p\cdots C(O)$	1.76	1.81	1.74	1.79	1.76	1.80
$Fe_p\cdots C(N^-)$	1.92	1.96	1.91	1.95	1.93	1.96
$Fe_d\cdots S_{\mu_1}$	2.33	2.37	2.34	2.40	2.38	2.40
$Fe_d\cdots S_{\mu_2}$	2.34	2.40	2.35	2.41	2.42	2.41
$Fe_d\cdots C(O)$	1.76	1.81	1.77	1.80	1.76	1.80
$Fe_d\cdots C(N^-)$	1.93	1.96	1.93	1.96	1.93	1.96
$Fe_p\cdots S_{\mu_b}$	2.44	2.43	2.43	2.50	2.52	2.60
$Fe_p\cdots C(CO_\mu)$	1.90	1.91	—	—	—	—
$Fe_d\cdots C(CO_\mu)$	2.08	2.16	—	—	—	—
$Fe_p\cdots O(O_2)$	—	—	1.93	1.97	1.86	1.91
$Fe_d\cdots O(O_2)$	—	—	2.01	1.99	1.97	1.97
			angles			
$Fe_p-S_{\mu_b}-Fe_1$	124.2	130.9	124.9	126.2	124.9	128.0
$Fe_4-Fe_1-S_{\mu_b}-Fe_p$	−80.1	−69.9	−85.0	−90.3	−88.4	−90.9

[a] The overall charge of the structural models is −3 elementary charges in each case. Structures were optimized using the TZVP basis set.

geometrical deviations between the structures optimized with BP86 and B3LYP do not lead to significant energetical changes for BP86. Strikingly, the small functional-induced structural changes for adducts **2b**−$[Fe_p(II)Fe_d(II)]^{3-}$ and **2c**−$[Fe_p(II)Fe_d(II)]^{3-}$ led to large deviations in the reaction energies for B3LYP. Obviously, B3LYP is more sensitive to the structural changes than BP86.

Because of these discrepancies and the extreme sensitivity of the calculations performed with B3LYP to the size of the basis set, we consider the BP86 functional to be better suited to describe the energetics of the reaction between dioxygen and the H-cluster of [FeFe]-hydrogenase. However, in all our conclusions, we take this variance into account in order to have them affected as little as possible by the unavoidable DFT inherent errors.

In order to analyze the specificity of O_2 addition to the H-cluster, we additionally considered O_2 to react with the iron and sulfur atoms of the $[Fe_4S_4]$ cluster, with the bridging S_μ atom of Cys_{503} and the sulfur atoms of the dithiolate ligand (not shown). For all these variants, the oxygen molecule dissociated from the cluster during structure optimization, thereby leaving its integrity unchanged. This indicates that the observed interaction of dioxygen with the distal Fe_d is specific.

7. Protonation and/or Reduction?

Starting with the O_2 adducts **2a**−$[Fe_p(II)Fe_d(II)]^{3-}$, **2b**−$[Fe_p(II)Fe_d(II)]^{3-}$, and **2c**−$[Fe_p(II)Fe_d(II)]^{3-}$, we investigate possible pathways explaining the irreversible inhibition of the binuclear cluster. For this, we consider a stepwise protonation of the bound O_2 molecules in the three binding modes described above (Figure 6) along with and without electron transfer to the cluster. If no reduction is considered, then the process of protonation consequently leads to an incremental increase of the charge of the H-cluster. The energetics of protonation was studied by considering the transfer of an external solvated proton to the different O_2 adducts. Because residue Cys_{299} is discussed to be involved in proton transport to the active site of [FeFe]-hydrogenase, we additionally determined the energy needed for transferring a proton from this side chain to each isomer. This was achieved by performing geometry optimizations with both protonated and deprotonated Cys_{299}. For the reduction steps, an isolated electron without kinetic energy was considered, and the reaction energies were obtained directly from the differences in energy of the reduced and oxidized species.

Table 8. Reaction Energies for the Formation of the O_2-Adducts **2a,b,c**−$[Fe_p(I)Fe_d(II)]^{4-}$ from **1a**−$[Fe_p(I)Fe_d(I)]^{4-}$ Based on Structure Optimizations with BP86/TZVP[a]

	2a	2b	2c
1a−$[Fe_p(I)Fed(I)]^{4-}$ + O_2 → **2a,b,c**	−67.6	−11.3	−20.5

[a] Energies are given in kcal/mol.

Table 9 shows for each compound studied that both protonation steps are highly exothermic. In all cases, the transfer of the first proton is energetically more favorable and does not induce severe structural changes for the O_2 adducts **2a**−$[Fe_p(II)Fe_d(II)]^{3-}$ and **2b**−$[Fe_p(II)Fe_d(II)]^{3-}$ (products **3a**−$[Fe_p(II)Fe_d(III)]^{2-}$ and **3b**−$[Fe_p(II)Fe_d(III)]^{2-}$ in Figure 8a and c). The length of the O−O-bond corresponds here to a peroxo species (Table 5, experimental value for BaO_2: 1.49 Å,[54] theoretical value for ferric-hydroperoxo species in Compound I: 1.46 Å[52]), which means that the cluster is oxidized by one electron. For isomer **2c**−$[Fe_p(II)Fe_d(II)]^{3-}$, the protonation of the oxygen atom bound to Fe_d (O_d) is more exothermic and results in the breaking of the O−O bond. This form is called **3c**−$[Fe_p(II)Fe_d(II)]^{3-}$ in the following — the other protonation product, where a proton is added to the oxygen atom close to Fe_p, **3d**−$[Fe_p(II)Fe_d(III)]^{2-}$, correspondingly.

It must be noted that the external protonation energies depend on the energy assumed for a solvated proton and must, therefore, be considered carefully. The energies for the internal proton transfer from Cys_{299} are more reliable and show that the first step is slightly endothermic for the formation of **3a**−$[Fe_p(II)Fe_d(III)]^{2-}$ and **3b**−$[Fe_p(II)Fe_d(III)]^{2-}$ (Table 9). Hence, it is not unlikely that this residue could act as the primary proton donor. For the protonation products **3c**−$[Fe_p(II)Fe_d(III)]^{2-}$ and **3d**−$[Fe_p(II)Fe_d(III)]^{2-}$ however, the endothermicity of proton transfer from Cys_{299} is more pronounced. In all cases, the high negative charge of the cluster of −3 elementary charges is not changed by this process and there should be a high proton affinity of Cys_{299}, as is qualitatively reflected by the large exothermic protonation energies calculated in reference to a solvated proton.

Interestingly, after transferring a second H^+ the two variants, featuring a freely accessible terminal oxygen atom, (**3a**−$[Fe_p(II)Fe_d(III)]^{2-}$ and **3a**−$[Fe_p(II)Fe_d(III)]^{2-}$) underwent cleavage of the O−O bond and water release upon structure optimization (products **4a**−$[Fe_p(II)Fe_d(IV)]^-$ and **4b**−$[Fe_p(II)Fe_d(IV)]^-$ in Figures 8b and d). When no reduction is considered, the cluster is again oxidized by this process. This corresponds formally to a $[Fe_p(II)$-$Fe_d(IV)]$ pair at the $[2Fe]_H$ subsite. In the case of the isomers

(54) Abrahams, S. C.; Kalnajs, J. *Acta Crystallogr.* **1954**, *7*, 838–842.

Table 9. Protonation Energies of the O_2-Adducts of [FeFe]-Hydrogenase in kcal/mol[a]

educt	external protonation (addition of H^+)[b]	internal protonation (H^+ from Cys_{299})
2a−$[Fe_p(II)Fe_d(II)]^{3-}$	−159.3	2.7
2b−$[Fe_p(II)Fe_d(II)]^{3-}$	−163.0	0.3
2c−$[Fe_p(II)Fe_d(II)]^{3-}$ to **3c**	−152.6	17.0
2c−$[Fe_p(II)Fe_d(II)]^{3-}$ to **3d**	−146.4	14.9
2a−$[Fe_p(II)Fe_d(II)]^{4-}$	−232.4	−14.9
2b−$[Fe_p(II)Fe_d(II)]^{4-}$	−235.3	−22.0
2c−$[Fe_p(II)Fe_d(II)]^{4-}$ to **3c**	221.3	[c]
2c−$[Fe_p(II)Fe_d(II)]^{4-}$ to **3d**	−217.2	77.9
3a−$[Fe_p(II)Fe_d(II)]^{2-}$	−109.6[d]	−5.6[d]
3b−$[Fe_p(II)Fe_d(II)]^{2-}$	−128.1[d]	−24.1[d]
3c−$[Fe_p(II)Fe_d(II)]^{2-}$	−97.9	−4.1
3d−$[Fe_p(II)Fe_d(II)]^{2-}$	−104.0	−10.2
3a−$[Fe_p(II)Fe_d(II)]^{3-}$	173.1	−5.6[d]
3b−$[Fe_p(II)Fe_d(II)]^{3-}$	193.1	−5.0[d]
3c−$[Fe_p(II)Fe_d(II)]^{3-}$	173.5	[c]
3d−$[Fe_p(II)Fe_d(II)]^{3-}$	−182.4	−20.3

[a] Data were calculated from energies of optimized structures obtained with BP86/TZVP. Protonated forms that result from external protonation have a charge of −2 elementary charges for the first and −1 elementary charges for the second protonation step, and products from internal protonation have a charge of −3 and −2 elementary charges, respectively. [b] Protonation energies were calculated by assuming for a solvated proton an energy of −262.4 kcal/mol.[36,37] [c] Cluster **3c**−$[Fe_p(II)Fe_d(II)]^{3-}$ dissociates upon structure optimization. [d] Protonation of **3a** and **3b** leads to water dissociation.

3c−$[Fe_p(II)Fe_d(III)]^{2-}$ and **3d**−$[Fe_p(II)Fe_d(III)]^{2-}$, both emerging hydroxo groups remain bound to the cluster during optimization (isomer **4c**−$[Fe_p(II)Fe_d(IV)]^-$ in Figure 8f).

Due to the water release upon formation of the isomers **4a**−$[Fe_p(II)Fe_d(IV)]^-$ and **4b**−$[Fe_p(II)Fe_d(IV)]^-$, no real protonation energies can be given in these cases. The whole process is highly exothermic if external proton transfer is considered and still exothermic if one assumes initial proton transfer from Cys_{299}. The largest contribution to the reaction energy would, thereby again, stem from reprotonation of the negatively charged Cys_{299}. A pure proton transfer process is observed for **4c**−$[Fe_p(II)Fe_d(IV)]^-$ where no water release takes place. In contrast to the first protonation, the transfer of the second proton from Cys_{299} obviously is also exothermic in these cases (starting from each of the two possible singly protonated educts). For both protonation schemes considered, the most exothermic reaction is the formation of isomer **4b**−$[Fe_p(II)Fe_d(IV)]^-$.

Structure optimization, after removal of the water molecules, does not change the geometry of the clusters significantly for isomer **4a**−$[Fe_p(II)Fe_d(IV)]^-$, and it turned out that product **4a**−$[Fe_p(II)Fe_d(IV)]^-$, with a terminally bound oxygen atom, is more stable than that of the μ-bridged isomer **4b**−$[Fe_p(II)Fe_d(IV)]^-$ by about 39 kcal/mol (BP86/TZVP). With 1.67 Å, the Fe_d−O distance in the optimized structure correlates well with DFT calculations on Compound I[55,56] (1.65 Å) and with an experimentally determined value of 1.65 Å measured for a nonheme Fe(IV)=O complex,[57] thereby corroborating a formal oxidation state of +IV for Fe_d.

In sharp contrast to the protonation, a reduction of the oxygenated cluster is, with values around 100 kcal/mol, energetically highly unfavorable (see Table 10). Similarly, the direct reduction of the active oxidized form of the H-cluster is of the same order. The high endothermicity may, to some extent, be due to the fact that an isolated system is considered in this study, and consequently, there occurs no partial charge compensation by the environment. However, with more than 25 kcal/mol even, for the singly protonated species, electron transfer is impeded from an energetic viewpoint. Unlike for the singly protonated compounds, all reaction products of the 2-fold proton transfer can readily be reduced as Table 10 shows. The transfer of a second electron, however, is highly unfavorable (Table 10). Whereas the direct reduction of the active oxidized form of the H-cluster is highly impeded, the addition of O_2 to the reduced H-cluster in state $[Fe_p(I)Fe_d(I)]$ shows almost the same exothermic energetics as for the oxidized form (see Table 8), implying that the reduced H-cluster, which is discussed to be an intermediate of the catalytic cycle,[19] should readily react with dixoygen. Furthermore, protonation of the emerging species turns out to be highly favorable by more than −170 kcal/mol for the transfer of a first and by more than −210 kcal/mol for the transfer of a second proton (Table 9).

8. CO_2 Ejection and Another Round of Dioxygen Addition?

Based on the reaction energies of initial O_2 addition and in view of the relative energies of the reaction products, the most likely process in oxygen-induced inactivation involves the formation of compound **4a**−$[Fe_p(II)Fe_d(IV)]^-$ with an oxygen atom bound to the distal Fe_d. Basically, two scenarios can be thought of, starting from the configuration in Figure 9. The first one involves protonation of the terminally bound oxygen (Figure 9). If a free solvated proton is considered, then this process is energetically highly favored by −45.2 kcal/mol (BP86/TZVP). This is followed by an exothermic reduction of the cluster (−79.8 kcal/mol). Alternatively, the cluster could be reduced first (−30.9 kcal/mol) and subsequently protonated (−94.1 kcal/mol).

As an alternative reaction path, we consider a modified starting structure in which the terminal oxygen atom of **4a**−$[Fe_p(II)Fe_d(IV)]^-$ is manually distorted toward the former bridging CO ligand (Figure 9). Interestingly, upon structure optimization, CO_2 is formed by an intramolecular reaction of the terminal oxygen atom with CO (lower panel of Figure 9). Although with − 23.0 kcal/mol (BP86/TZVP), this process is less favorable than reduction and protonation; it implies the possibility of a further round of O_2 addition to the H-cluster again followed by protonation and water abstraction. We considered different possible sequences of events with high exothermicity, as depicted in Figure 10. We shall note again that the assignment of oxidation numbers is

(55) Schöneboom, J. C.; Neese, F.; Thiel, W. *J. Am. Chem. Soc.* **2005**, *127*, 5840–5853.

(56) Zheng, J.; Wang, D.; Thiel, W.; Shaik, S. *J. Am. Chem. Soc.* **2006**, *128*, 13204–13215.

(57) Rohde, J.-U.; In, J.-H.; Lim, M. H.; Brennessel, W. W.; Bukowski, M. R.; Stubna, A.; Münck, E.; Nam, W.; Que, L. *Science* **2003**, *299*, 1037–1039.

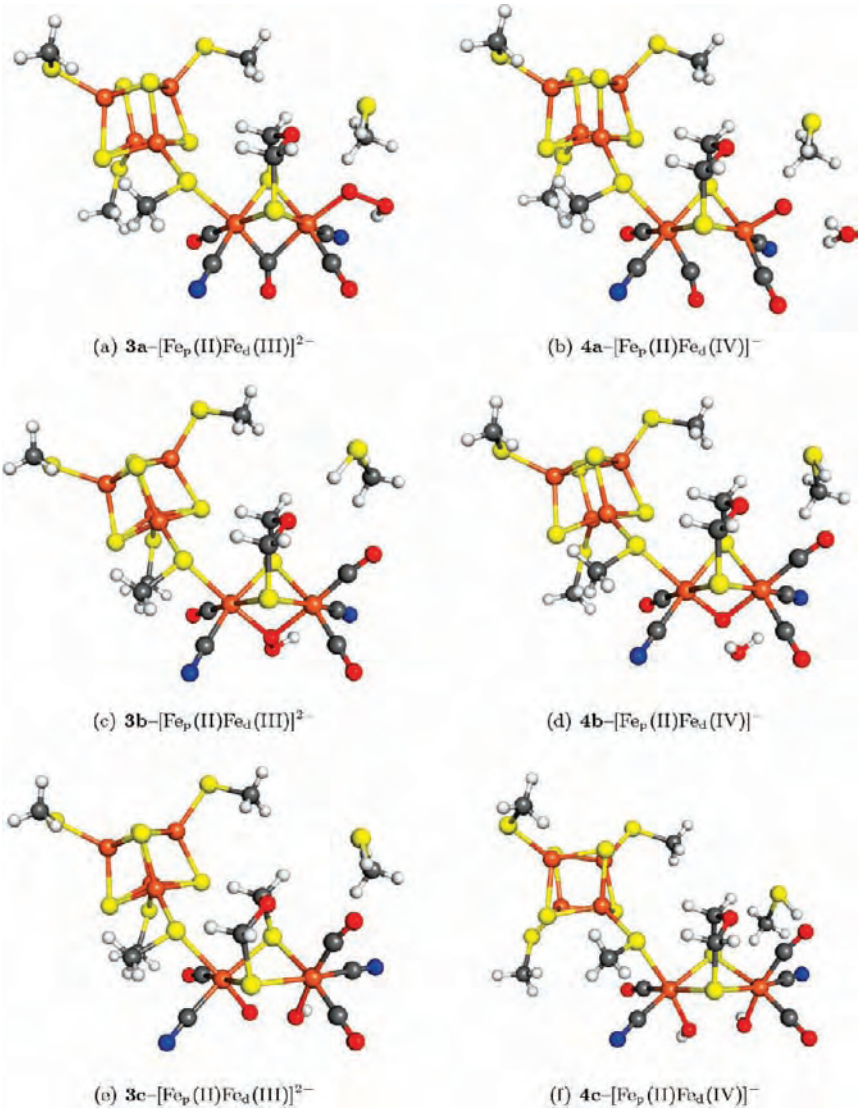

Figure 8. Protonation products of dioxygen adducts of [FeFe]-hydrogenase. *Left panel*: Optimized structures (BP86/TZVP) after transfer of one proton to the O_2 adducts shown in Figure 6. The charge is −2 elementary charges in each case. *Right panel*: Optimized structures (BP86/TZVP) after transfer of one proton to the singly protonated species. The charge is −1 elementary charges in each case.

Table 10. Reduction Energies in kcal/mol for Different Forms of the H-cluster of [FeFe]-Hydrogenase[a]

	reduction energy	
educt	1st e$^-$	2nd e$^-$
1a−[Fe$_p$(I)Fe$_d$(II)]$^{3-}$	102.6	—
1b−[Fe$_p$(I)Fe$_d$(II)]$^{3-}$	102.7	—
2a−[Fe$_p$(II)Fe$_d$(II)]$^{3-}$	99.5	—
2b−[Fe$_p$(II)Fe$_d$(II)]$^{3-}$	104.6	—
2c−[Fe$_p$(II)Fe$_d$(II)]$^{3-}$	99.1	—
3a−[Fe$_p$(II)Fe$_d$(III)]$^{2-}$	26.4	—
3b−[Fe$_p$(II)Fe$_d$(III)]$^{2-}$	31.1	—
3c−[Fe$_p$(II)Fe$_d$(III)]$^{2-}$	25.6	—
3d−[Fe$_p$(II)Fe$_d$(III)]$^{2-}$	28.3	—
4a−[Fe$_p$(II)Fe$_d$(IV)]$^{-}$	−37.1	30.0
4b−[Fe$_p$(II)Fe$_d$(IV)]$^{-}$	−39.8	25.7
4c−[Fe$_p$(II)Fe$_d$(IV)]$^{-}$	−50.0	26.5

[a] Data were calculated from energies of optimized structures obtained with BP86/TZVP.

difficult (i.e., often not unambiguously possible), especially for the highly oxidized species shown in Figure 10; we use the oxidation number assignment mainly for labeling purposes.

Apparently, all steps are highly favorable and compared with the formation of the hydroxylated and reduced species **5**−[Fep(II)Fed(III)]$^-$, the energy gain of this pathway would be significantly higher. It is possible to enter this reaction path with an initial reduction step of the CO_2 deprived structure **4a**−[Fe$_p$(II)Fe$_d$(IV)]$^-$ with an energy gain of −28.3 kcal/mol. With − 45.3 kcal/mol, the addition of O_2 to this form is even more exothermic than for the oxidized one. If no reduction takes place at all, then the transfer of the second proton is no longer favored but slightly endothermic by 2.5 kcal/mol.

With an O−O bond length of 1.30 Å, the bound oxygen moiety of compound **6**−[Fe$_p$(II)Fe$_d$(IV)]$^-$ can be considered as a superoxide species (compare Section 7). Therefore, the cluster is oxidized by this process by 1 elementary charge. Interestingly, subsequent reduction leads to an interaction between the bound oxygen species and the nearby CO_2 molecule. The O−O bond increases to 1.47 Å, and the distance

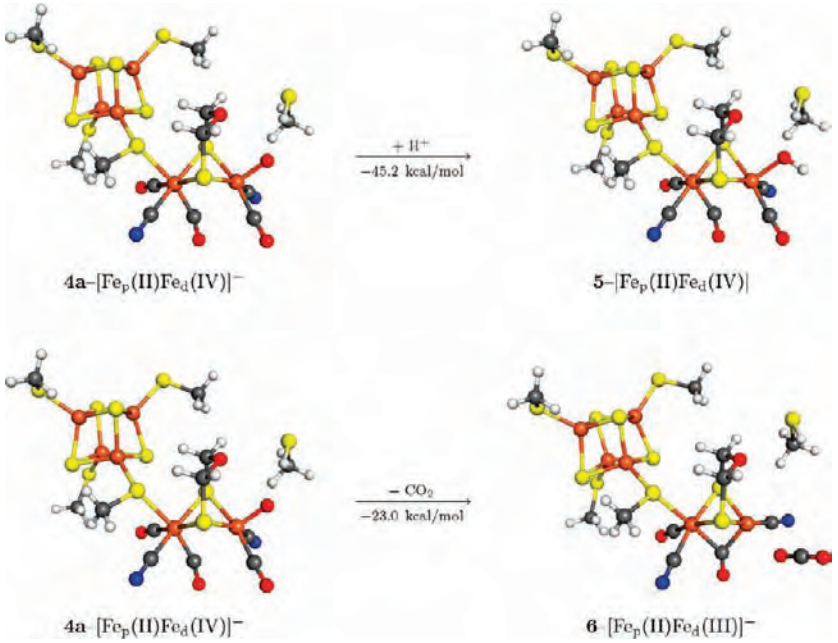

Figure 9. Alternative pathways for the terminally oxygenated H-cluster. *a*: Optimized structures (BP86/TZVP) for the protonation reaction of **4a**. Reaction energy was calculated by assuming an energy of −262.4 kcal/mol for a solvated proton.[36,37] *b*: Optimized structures (BP86/TZVP) for the CO_2 abstraction. Compound **6** was obtained after bending the terminal oxygen atom of **4a** toward the bridging CO ligand.

of the oxygen atom of CO_2 next to Fe_d shortens from 2.22 to 1.97 Å. By transferring a proton to the terminal oxygen atom, CO_2 is again released, and with 1.52 Å, the O−O bond length can be assigned to a peroxo state (see discussion in Section 7). The Fe_d−O bond length of the water deprived structures **8**−[Fe_p(II)Fe_d(V)] and **8**−[Fe_p(II)Fe_d(IV)]$^-$ is with 1.63 Å smaller than that of a Fe(IV)=O complex (1.65 Å, see Section 7) but still significantly longer than that of an experimentally determined Fe(V)−O bond (1.58 Å).[58] Therefore, it is reasonable to assume a redox state of +IV for both compounds.

Interestingly on the example of the water-deprived structure **8**−[Fep(II)Fed(V)], which was obtained by assuming a singlet state, we checked for higher spin states and found them to be only about 3 kcal/mol higher in energy. But apparently, high spin states are not preferred after destroying the ligand sphere of the Fe_d atom.

Regardless in which sequence the events take place, the repetitive addition of dioxygen followed by water abstraction is a highly exothermic process that can explain the irreversibility of dioxygen-induced inhibition of [FeFe]-hydrogenase by a systematical breakdown of the ligand sphere of the $[2Fe]_H$ subsite.

9. Discussion and Conclusion

Inhibition by dioxygen is a major drawback for the application of [FeFe]-hydrogenase in hydrogen fuel production or as electrocatalysts for hydrogen oxidation in fuel cells. By performing DFT calculations, we were able to uncover possible reaction pathways that can explain this process on a molecular level. Obviously, the energetics of [FeFe]-hydrogenase are difficult to describe accurately using DFT, and, in this respect, it is important to note that double-ζ basis sets are inadequate, especially in combination with the B3LYP functional.

Despite the large deviations of the reaction energies calculated for addition of dioxygen to the H-cluster, the functionals BP86 and B3LYP give qualitatively similar results with the TZVP basis set. This was further confirmed by calculations using the TPSS functional. Hence, the interaction of dioxygen with the active form of the H-cluster of [FeFe]-hydrogenase should be a highly exothermic and specific process. The most probable reaction product would, thereby, be a species in which O_2 is bound in an end-on way to the distal Fe-atom of the $[2Fe]_H$ subsite. This resembles the typical binding mode of dioxygen to the heme-Fe(II) center in Cytochrome P450.[52] Interestingly, Baffert et al. provided experimental evidence that O_2 should indeed interact in a specific manner with the H-cluster. With kinetic measurements on [FeFe]-hydrogenase from *Clostridium acetobutylicum*, they showed that the enyzme can be protected from O_2 inactivation by the competitive inhibitor CO that binds to the active site of the enzyme.[7] However, EPR measurements on the *Desulfovibrio vulgaris* hydrogenase indicate oxidative damage of auxiliary [Fe_4S_4] clusters upon air exposure. Therefore, additional mechanisms may exist that contribute to O_2-induced inhibition and depend on the species origin of the enzyme studied.[6]

Based on the energetics calculated, it is tempting to propose a protonation mechanism for the terminal oxygen atom of the attached O_2 molecule. This leads to water abstraction from the cluster, which could contribute to the irreversibility of enzyme inactivation. The protonation of all three compounds under investigation turned out to be highly energetically favored.

In the present study, we did not account for the detailed mechanisms of proton transfer. Cys_{299}, which we included in our model systems, is often mentioned as a possible proton shuttle during the catalytic cycle of [FeFe]-hydrogenase [41].

(58) de Oliveira, F. T.; Chanda, A.; Banerjee, D.; Shan, X.; Mondal, S.; L., Q. Jr.; Bominaar, E. L.; Münck, E.; Collins, T. J. *Science* **2007**, *315*, 835–838.

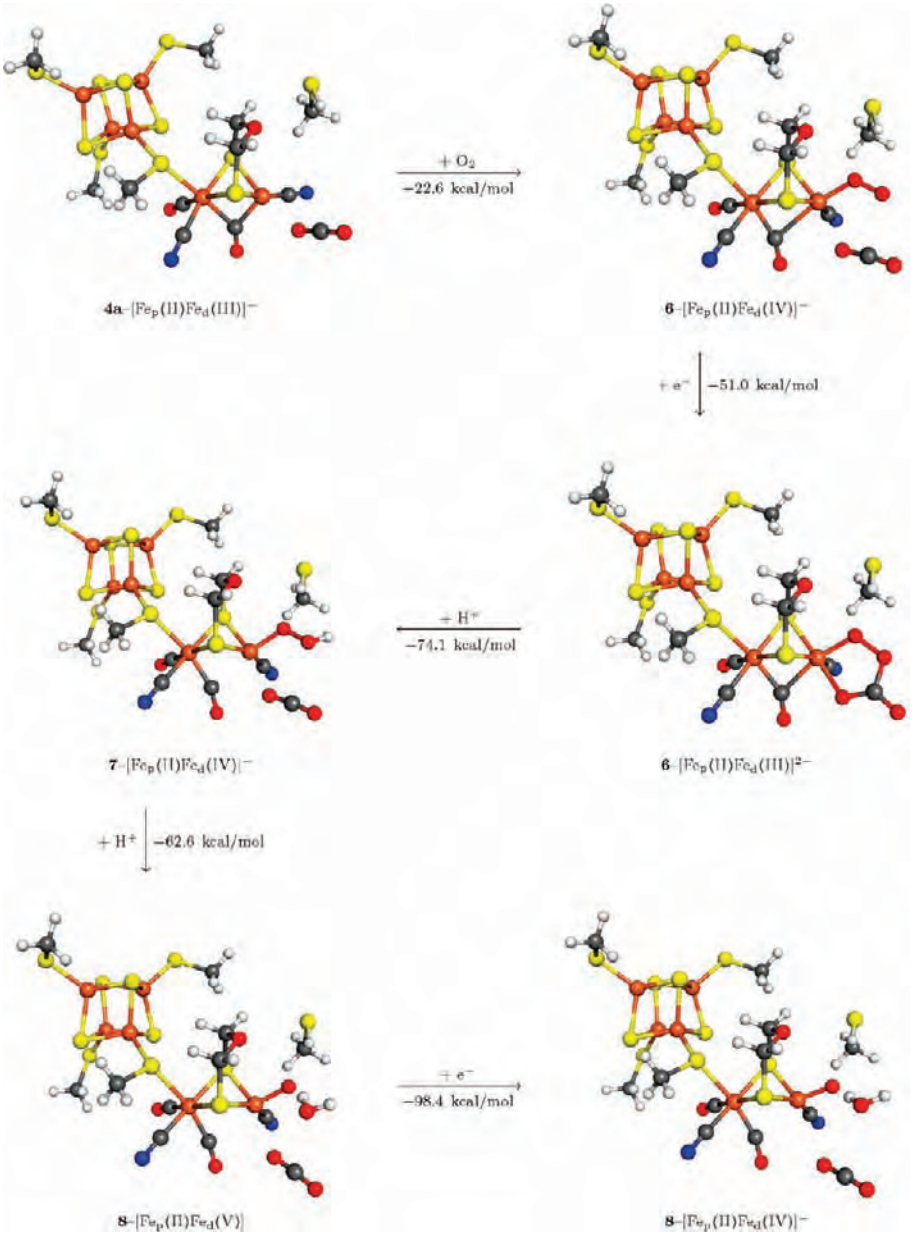

Figure 10. Reaction path starting from the CO_2 deprived structure **4a**−$[Fe_p(II)Fe_d(IV)]^-$. Structures optimized with BP86/TZVP. Oxidation numbers are used for labeling purposes and have to be taken with care, especially for the highly oxidized species.

However, we did not observe proton transfer from this residue to either the bridge-head atom or to any of the terminally bound oxygen species during geometry optimizations. This was also not the case for calculations on the terminal O_2 adduct in which the bridging oxygen atom was substituted by an NH group (not shown). Therefore, we studied the proton transfer fom Cys_{299} to dioxygen species bound to the $[2Fe]_H$ subcluster. It turned out that this process is thermodynamically slightly unfavorable for each of the studied oxygen adducts. However, with 2.7 and 0.3 kcal/mol, the endothermicity of the reaction is only small for protonation of the compounds **3a**−$[Fe_p(II)Fe_d(III)]^{2-}$ and **3b**−$[Fe_p(II)Fe_d(III)]^{2-}$, and a direct proton transfer from Cys_{299} is, therefore, not unlikely in these cases. Clearly, the high exothermicity calculated by assuming the transfer of a solvated proton is certainly due to charge compensation at the negatively charged cluster. For future work, it will be interesting to assess these protonation energies in a more balanced model, including the protein environment and explicit water molecules using a QM/MM approach.

The multiple-step mechanism we describe here agrees well with the experimental results of Baffert et al.[7] Based on kinetic measurements performed with [FeFe]-hydrogenase isolated from *Clostridium acetobutylicum*, they proposed that enzyme inactivation takes place by the initial reversible formation of an O_2 adduct followed by an irreversible modification of the active site. Calculations on the H-cluster, after protonation and water abstraction, suggest a stable reaction product with a $[Fe_p(II)Fe_d(IV)]$ pair at the $[2Fe]_H$ subsite. In this state, the cluster would be more highly oxidized than the inactive but reducible form of H_{ox}^{inact} that was experimentally characterized and which, most likely, corresponds to a $[Fe_p(II)Fe_d(II)]$ site.[59] It is very intriguing

(59) Greco, C.; Bruschi, M.; Heimdal, J.; Fantucci, P.; De Gioia, L.; Ryde, U. *Inorg. Chem.* **2007**, *46*, 7256–7258.

that inactivation of [FeFe]-hydrogenase by O_2 can be reverted if the enzyme is oxidized under anaerobic conditions prior to oxygen contact.[2] In its inactive form, the enyzme is obviously insensitive against O_2. This is in line with our calculations, which suggests that the formation of an oxygen adduct is exothermic for the active oxidized form H_{ox}^{cat}, whereas we found only a small favorable reaction energy of −14.5 kcal/mol (BP86/TZVP) for the attachement of O_2 to the distal Fe_d in oxidation state +II.

In a QM/MM study on the inhibition of the H-cluster, Dogaru et al. considered the addition of O_2 to the distal Fe_d atom and showed that, in a similar series of events as discussed in the present work, an end product emerges with one oxygen atom bound to the terminal Fe_d atom. The authors claim that a hydroxylated species of the H-cluster is obtained via a fully exergonic pathway and that this compound would correspond to the end product of the inhibition process. However, especially for the enzyme variant from *Desulvovibrio desulfuricans*, which is completely inactivated by O_2, it is unlikely that the irreversibility of this process can be explained by formation of this product alone.

We also considered the possibility of reduction and protonation of compound **4a**−$[Fe_p(II)Fe_d(IV)]^-$ with an terminal oxygen atom bound to the distal Fe_d atom and found that both steps are highly exothermic, like all reaction steps leading to this species. However, further reduction of the product that would result in the compound described by Dogaru et al. is endothermic in our case.

Clearly, further addition of dioxygen after CO_2 ejection from the $[2Fe]_H$ subsite, as presented here, represents a tempting reaction mechanism that can account for the irreversibility of dioxygen-induced inhibition of [FeFe]-hydrogenase. We have shown that by rereducing the oxidized CO_2 deprived H-cluster, the sequence of events leading from O_2 addition to water release can take place for a second time. Indeed, one could imagine a mechanism with a stepwise decomposition of the ligand environment of the H-cluster and, consequently, its destruction.

For subsequent work, it will be important to study reaction barriers for the crucial reaction steps, especially for the bending of the terminal oxygen atom of compound **4a**−$[Fe_p(II)Fe_d(IV)]^-$ in order to quantify the likeliness of alternative reaction paths. Such investigations are in progress in our laboratory.

Acknowledgment. We would like to thank Prof. Luca De Gioia and his group for stimulating discussions concerning the chemistry of hydrogenase. This work has been financially supported by ETH Zurich and the Schweizer Nationalfonds (project no. 200020−121870).